Direct Visualization of Catalytically Active Sites at the FeO–Pt(111) Interface

Wilhelmine Kudernatsch,[†] Guowen Peng,[‡] Helene Zeuthen,[†] Yunhai Bai,[‡] Lindsay R. Merte,[†] Lutz Lammich,[†] Flemming Besenbacher,[†] Manos Mavrikakis,[*,‡] and Stefan Wendt[*,†]

[†]Interdisciplinary Nanoscience Center (iNANO) and Department of Physics and Astronomy, Aarhus University, DK-8000 Aarhus C, Denmark and [‡]Department of Chemical and Biological Engineering, University of Wisconsin-Madison, Madison, Wisconsin 53706, United States

ABSTRACT Within the area of surface science, one of the "holy grails" is to directly visualize a chemical reaction at the atomic scale. Whereas this goal has been reached by high-resolution scanning tunneling microscopy (STM) in a number of cases for reactions occurring at flat surfaces, such a direct view is often inhibited for reaction occurring at steps and interfaces. Here we have studied the CO oxidation reaction at the interface between ultrathin FeO islands and a Pt(111) support by *in situ* STM and density functional theory (DFT) calculations. Time-lapsed STM imaging on this inverse model catalyst in O_2 and CO environments revealed catalytic activity occurring at the FeO–Pt(111) interface and directly showed that the Fe-edges host the catalytically most active sites for the CO oxidation reaction. This is an important result since previous evidence for the catalytic activity of the FeO–Pt(111) interface is essentially based on averaging techniques in conjunction with DFT calculations. The presented STM results are in accord with DFT+U calculations, in which we compare possible CO oxidation pathways on oxidized Fe-edges and O-edges. We found that the CO oxidation reaction is more favorable on the oxidized Fe-edges, both thermodynamically and kinetically.

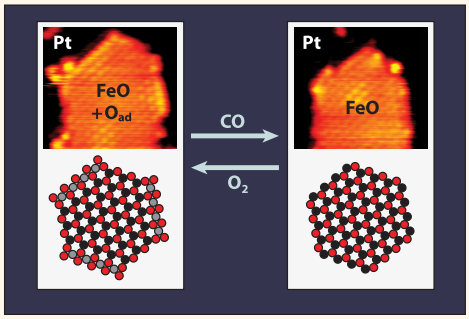

KEYWORDS: catalysis · active sites · CO oxidation · FeO islands · Pt · *in situ* scanning tunneling microscopy (STM) · density functional theory (DFT)

The identification of active sites in heterogeneous catalysis is essential for a basic understanding of the reaction mechanism(s), which is crucial for improving the properties of industrial catalysts. Active sites of a catalyst surface can be regular, under-coordinated terrace sites,[1−4] but most frequently proposed have been defect sites such as step edges, kinks and point defects.[4−14] On one hand, the step edges on the actual catalytically active material, such as Pt, Ru, Pd or Au particles have been found to be highly relevant.[4−6,8,9,15−17] On the other hand, since heterogeneous catalysts are typically composed of several components such as metal particles (usually noble metals or alloys of them) and a support (usually metal oxides), the interfaces between these components are also possible hosts of the active sites. Several examples are known today, where the reactivity is largest at the interface between metal nanoparticles and the oxide support.[12,13,18−20]

Because heterogeneous catalysts are complex materials and the reaction conditions are usually very harsh, the study of active sites is often undertaken by using the so-called surface science approach. In this approach, a heterogeneous catalyst is reduced to its basic components and studied under well-controlled conditions, often in ultrahigh vacuum (UHV).[21−23] The great advantage of this approach is that the full pallet of surface science tools can be utilized, including both averaging spectroscopy and scanning probe microscopy techniques, with scanning tunneling microscopy (STM) being the most widely used imaging technique.

STM studies have often been very insightful for the identification of catalytically active sites, particularly when these sites are located on the terraces.[23−27] For example, Wintterlin et al. have imaged adsorbed O atoms and CO molecules on Pt(111), and monitored their reaction to carbon dioxide

* Address correspondence to emavrikakis@wisc.edu, swendt@phys.au.dk.

Received for review April 19, 2015 and accepted May 31, 2015.

Published online May 31, 2015
10.1021/acsnano.5b02339

(CO_2) as a function of time.[24] On the basis of the observed microscopic mechanism, these authors succeeded to extract quantitative rate laws from the atomically resolved surface processes, that is, to derive the reaction kinetics. With the most stable scanning tunneling microscopes, it is indeed possible to visualize dynamic processes on surfaces by recording time-resolved sequential STM images in the form of so-called STM-movies.[24,28−34]

However, when step edges come into play, the utilization of several experimental techniques is often mandatory,[4,10,12,13,17,35−39] because the interpretation of STM images of step edges and interfaces is not straightforward.[15,36,38,40,41] Thus, the visualization of catalytic activity at step edges directly by STM remains a challenge. As a result, to infer on the activity of step edges, it is frequently the *lack of activity* that can be evidenced when the active sites at step edges are blocked. For example, on a Ru(0001) single crystal, the dissociation of N_2 molecules can be quenched by decorating the steps with Au.[6] Similarly, on rutile TiO_2(110), the dissociation of water was found to be diminished when the step edges were blocked by ethoxy species.[42] These examples illustrate why the evidence for catalytic activity at step edges has often been based essentially on averaging techniques in combination with DFT calculations.

In the present work, we report on the active sites of Pt(111)-supported, two-dimensional FeO islands in the CO oxidation reaction. This model catalyst, denoted in the following as FeO_{is}/Pt(111), was introduced by groups from Dalian and Hefei in 2010.[10,43] It is a so-called "inverse catalyst", where the oxide patches (partly) cover the metal particles.[18,44−47] In contrast to continuous, ultrathin FeO films on Pt(111), the FeO−Pt(111) interface is accessible, exposing under-coordinated atoms at the FeO island edges. This renders the FeO_{is}/Pt(111) model system more active in the CO oxidation reaction than bare Pt(111), as inferred from time-lapsed ultraviolet photoemission spectroscopy measurements at 273 K, STM measurements and accompanying DFT calculations.[10] The importance of the FeO−Pt(111) interface and coordinatively unsaturated ferrous (CUF) sites for the catalytic activity has been emphasized,[10,43,47−52] but *direct evidence* for the island edges as hosts of the active sites is still lacking.

Pt(111)-supported FeO nanoislands are composed of hexagonal Fe−O bilayer structures with the Fe layer between the Pt substrate and the terminating O layer,[10,43,53] exactly like in continuous FeO bilayer films on Pt(111).[54] In our recent STM study addressing FeO_{is}/Pt(111)[53] we reported that the FeO islands occur in two different FeO orientations that are characterized by a distinct positioning of the O lattice. The FeO edges are either predominantly Fe-terminated or O-terminated, depending on the applied preparation conditions

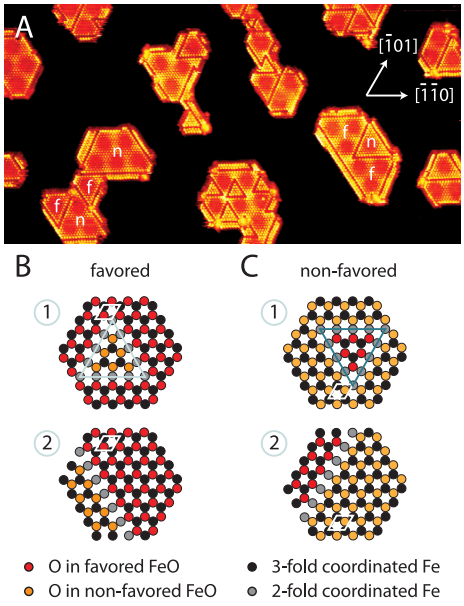

Figure 1. (A) STM image (550 Å × 290 Å) of O-poor FeO islands on Pt(111) with O vacancy dislocations. An as-prepared FeO_{is}/Pt(111) sample was annealed in 1.3 × 10^{-6} mbar O_2 at 475 K for 2 min, followed by H_2 exposure at RT (1.3 × 10^{-7} mbar, 2 min) and subsequently vacuum-annealed at 575 K for 1 min. The scanning conditions were I_t = 0.61 nA and V_t = 70 mV. On two islands, "f" and "n" indicate patches of FeO in favored and nonfavored orientation, respectively. (B, C) Models of hexagonal O-poor FeO islands on Pt(111) with the FeO being predominantly in favored (B) or nonfavored (C) orientation. Type (1) models are characterized by O vacancy dislocation loops and type (2) models by O vacancy dislocations along O-edges, transforming them into Fe-edges.

(reducing or oxidizing). Thus, in connection with changes of the island shapes, the structures of the edges change as well. In addition to the two edge types of pristine FeO islands, Fe- and O-edges, we have deduced the atomic structures of three further edge types:[53] (i) Oxidized Fe-edges that are formed by addition of O atoms to original Fe-edges at oxidizing conditions, (ii) O-edges that have formed at oxidizing conditions by inversion of the FeO between the boundary and O adatom dislocation lines on the island, and (iii) Fe-edges that have formed at reducing conditions by inversion of the FeO in a narrow ribbon (∼10 Å) between the boundary and an O vacancy dislocation line on the island (see further details below and in Figure 1A).

Here we present direct STM evidence that the active sites on FeO_{is}/Pt(111) in the CO oxidation reaction are indeed the CUF sites. Specifically, we show by *in situ* STM measurements at room temperature (RT) that CO oxidation occurs at oxidized Fe-edges, which are characterized by O adatoms along the original Fe-edges. Our DFT calculations addressing possible CO oxidation pathways at O-edges and oxidized Fe-edges are in accord with the STM results, showing that the CUF sites are indeed the most active sites on the FeO_{is}/Pt(111) model catalyst.

RESULTS

STM Results. Figure 1A depicts a high-resolution STM image of O-poor FeO islands on Pt(111), which was acquired in a tip-dependent imaging mode where the Fe atoms appear as protrusions.[55] This STM image was recorded after reactive deposition of Fe in a background of 1×10^{-6} mbar O_2 with the sample held at RT ["*as-prepared* FeO_{is}/Pt(111)"]. Subsequently, the FeO_{is}/Pt(111) sample with FeO islands covering ~25% of the surface was exposed to reducing conditions including vacuum-annealing at 575 K for 1 min (see Figure 1 for details). Accordingly, we expect the FeO islands to be dominated by Fe-rich edges, whereas O-terminated edges should be scarce and short.[53] Whereas the edge-terminations cannot be seen directly in the STM image, the moiré superstructure with the three high-symmetry domains [top, face-centered cubic (fcc), and hexagonal close-packed (hcp), denoted according to the stacking order of the atoms in each domain][54,56,57] can be recognized on the islands, and numerous O vacancy dislocations appearing as dark lines can be clearly seen as well. Many of these O vacancy dislocations are running parallel to the island edges, but triangular-shaped dislocations also frequently occur. Such O vacancy dislocations have previously been observed on both Pt(111)-supported continuous FeO films[56,58] and FeO islands[53] and described in great detail. Briefly, O vacancy dislocations form upon reduction of the FeO bilayer and the shifting of the remaining O atoms to adjacent hollow sites in the Fe lattice, which is driven by the different stability of FeO on the three high-symmetry domains.[56]

On the FeO islands in Figure 1A, most triangular O vacancy dislocations appear with their apexes pointing "up". Considering this orientation of the triangles with respect to the supporting Pt(111) sample,[53] we conclude that the FeO outside the triangles is in the favored orientation (see the indicated FeO orientations on two islands in Figure 1A and the models in Figure 1B,C). In the case of pristine FeO islands, ~75% of the islands consist predominantly of FeO in the favored orientation.[53] The long O vacancy dislocations running parallel to the edges create ~10 Å wide FeO ribbons along the edges that are inverted with respect to the FeO in the center parts of the islands. In this way, most of the (original) O-edges are converted to Fe-edges.

These inversions of the FeO are illustrated in the models depicted in Figure 1B,C, where we have drawn, for simplicity, hexagonal-shaped islands that are characterized by alternating Fe- and O-edges with identical length. Models labeled "1" exhibit triangular O vacancy dislocation loops. For both FeO orientations, the edges of these O dislocations are running parallel to the island Fe-edges. Models labeled "2" show O vacancy dislocation lines that are running parallel to one of the original O-edges, transforming it into a Fe-edge.

As a result, O vacancy dislocation lines are always running parallel to Fe-edges, and are thus clear indicators of the island's edge-termination.[53] Very similar considerations help identifying the edge-termination of O-rich FeO islands by means of O adatom dislocations (rows of additional O atoms) that appear at central regions and at the junctions of interconnected FeO islands.[53] In an analog way as O vacancy dislocations transform O-edges into Fe-edges, the O adatom dislocations lead to transformations of Fe-edges into O-edges. O adatom dislocations are therefore always running parallel to O-edges, regardless of the FeO orientation.[53] Taking additionally into consideration that adjacent edges exhibit opposing edge termination, the observation of an O dislocation line of either type allows the identification of all edges of a specific, considered island.

In our *in situ* STM measurements addressing CO oxidation on FeO_{is}/Pt(111) at RT (see Figures 2–4 and the movie on CO oxidation in the Supporting Information), the preparation of the Pt(111)-supported FeO islands was accomplished in a similar way as was done in the STM experiment illustrated in Figure 1. Specifically, an as-prepared FeO_{is}/Pt(111) sample was flash-annealed up to 600 K in UHV. Thus, reduced FeO islands can be expected, meaning that most island edges should be Fe-terminated. Indeed, the islands were characterized by O vacancy dislocation lines and loops, similar to the situation in Figure 1A. Additionally, because of the flash-anneal to 600 K quite large FeO islands resulted, with an average diameter of ~60 Å. Before the acquisition of the STM movie, the surface was exposed to CO at RT [~10 L (Langmuir), with 1 L = 1.33×10^{-6} mbar·s], which is sufficient to saturate the bare Pt(111) regions on the FeO_{is}/Pt(111) surface with CO.[59] This order of exposures (first CO, subsequently O_2) was chosen because the strongly bound CO molecules inhibit the dissociation of impinging O_2 molecules on the Pt(111) regions;[60,61] thus, the Pt-regions are passivated. Figure 2 shows selected STM images that were acquired within the STM movie, which was recorded during alternating O_2 and CO exposures with a rate of 40 s per image. In the STM movie, the state of the tip apex was such that original Fe-edges and oxidized Fe-edges (characterized by a row of O adatoms off the Fe-edge) could be distinguished by their apparent heights.

In Figure 2A (image #22 of the movie on CO oxidation), the surface was still saturated with CO, even though O_2 was dosed at pressures up to 6.4×10^{-8} mbar (in total ~25 L O_2) directly before this STM image was acquired. On the Pt(111) regions, the presence of CO is noticeable from the $c(4 \times 2)$-CO structure, which is expected following CO saturation at RT.[62,63] The few small circular depressions on Pt(111), some of which

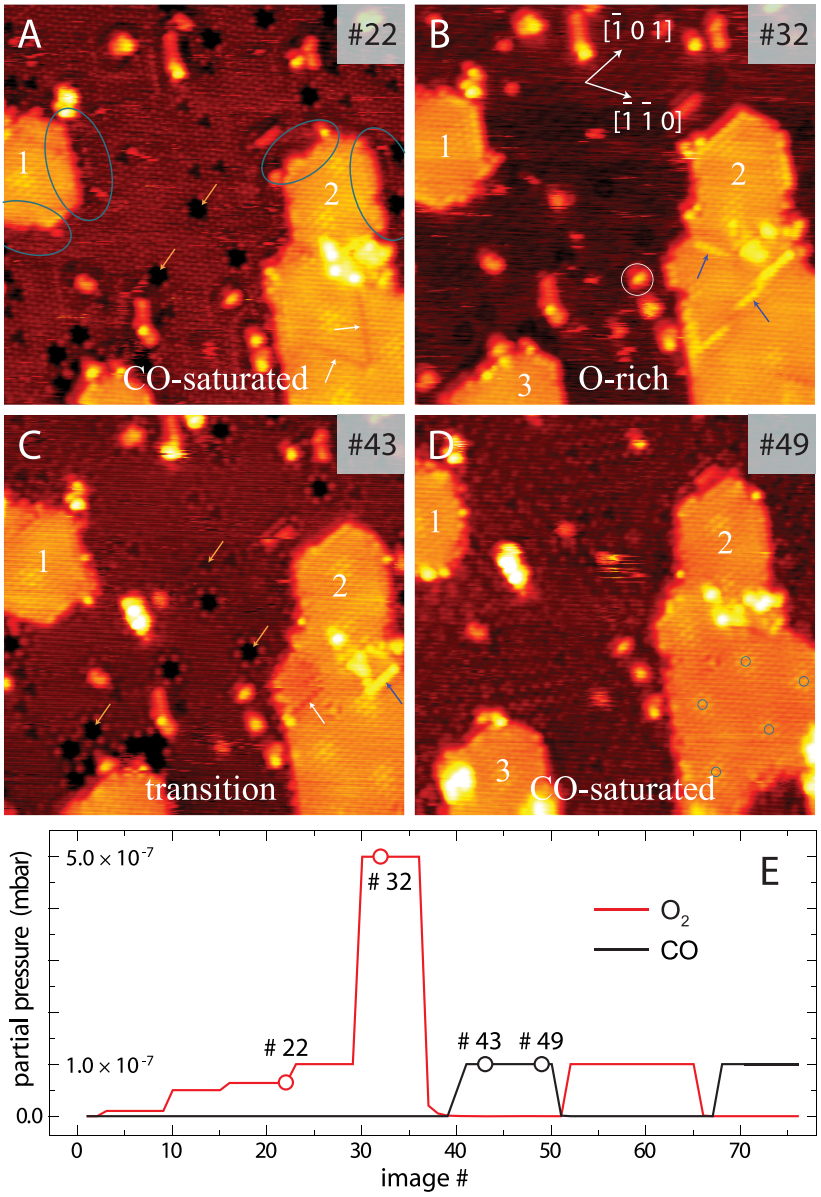

Figure 2. (A–D) Selected STM images (150 Å × 150 Å) acquired within the STM movie on CO oxidation at alternating O_2 and CO exposures at RT. The image numbers are indicated in the upper right corners. The starting situation was an as-prepared FeO_{is}/Pt(111) sample that was flash-annealed up to 600 K in UHV. Subsequently, the surface was saturated with ~10 L CO at RT. Three FeO islands labeled 1–3 were imaged. The focus is on the Fe-edges on islands 1 and 2 that are highlighted in (A) by ellipses. On island 2, white arrows indicate O vacancy dislocations and blue arrows O adatom dislocations. In (A) and (C), orange arrows indicate restructured regions on Pt(111) that can be formed in the presence of oxygen and subsurface Fe atoms.[64] In (D), blue circles indicate the top domains. The STM movie was recorded with a rate of 40 s per image at I_t = 0.31 nA and V_t = 593 mV. In (A), the surface was still saturated with CO, even though O_2 was dosed at pressures up to 6.4×10^{-8} mbar (in total ~25 L). Following additional O_2 exposures (~100 L) in (B), the Fe-edges became bright, indicating the oxidation of these edges. Further O_2 and subsequent CO exposures (C, ~9 L CO and D, additional ~25 L CO) led to the restoration of bare Fe-edges on island 1 and the upper end of island 2. (E) Background pressure conditions during the recording of the STM movie.

are marked by orange arrows, arise most likely from a restructuring induced by oxygen adsorption and subsurface Fe atoms.[64] In principle, such depressions could also arise from O adatom islands, since chemisorbed O atoms on Pt(111) also appear in STM images as depressions.[23,65,66] However, chemisorbed O atoms on Pt(111) are expected to react with CO at RT[24] and, thus, changes of these features should occur upon alternating O_2 and CO exposures if these were due to O adatom islands. Since we did not observe any changes on the circular depressions on the Pt(111) areas during the course of the STM movie we favor the former interpretation. With the exception of the small circular depressions, we can state that the Pt(111) areas in image #22 are covered by CO.

On the FeO islands, CO does not bind[67,68] and thus CO molecules cannot be present. Nevertheless, the presence of O vacancy dislocation lines on island 2

(marked by white arrows in Figure 2A) indicates that the island was in a reduced state, which is consistent with the presence of CO molecules on the Pt(111) areas. Note that the partial pressures measured in the vacuum chamber can differ considerably from the partial pressures at the sample surface, since the geometry of the Aarhus-STM instrument hinders efficient pumping of the sample surface region during STM experiments. Therefore, changes made to the overall gas environment can be both attenuated and delayed at the sample surface.

Figure 2B shows STM image #32 of the movie on CO oxidation. In this image, clear signs are seen that additional O_2 exposure (~100 L O_2) led to O-rich conditions on the surface. Several changes are noticeable in image #32 (Figure 2B) compared to image #22 shown in Figure 2A. On FeO island 2, the dark O vacancy dislocation lines disappeared and new bright O adatom dislocations appeared instead (some are marked by blue arrows). In addition, several edges on islands 1 and 2 (marked by ellipses in Figure 2A) appeared much brighter, indicating that reactions had occurred at these island edges due to additional O_2 exposure. In the Pt(111) regions, the STM contrast is fuzzy and no clear structure can be recognized.

In the further course of the STM movie the O_2 exposure was continued, but starting from image #39 the O_2 leak valve was closed, and instead the FeO_{is}/Pt(111) sample was exposed to CO. The next two STM images (#43 and #49 presented in Figure 2C and D) were acquired during CO exposure (1.0×10^{-7} mbar in the chamber). The transition from an O-rich to a CO-saturated situation is seen in image #43, where island 2 shows O adatom and O vacancy dislocations at the same time. Note also that the four island edges that are marked by ellipses in Figure 2A appear no longer particularly bright in the STM image. Finally, in image #49, all the O adatom dislocations seen in image #32 at O-rich conditions are absent and no sign of enhanced apparent height is seen at all at the island edges. In all four cases the enhanced apparent edge height could be recovered by dosing O_2 again (see the movie on CO oxidation). Regarding image #49 in Figure 2D we note that the $c(4 \times 2)$-CO structure on the Pt(111) regions could be recognized again.

On the basis of the uppermost O adatom dislocation line defect on island 2 in image #32 (see Figure 2B), it is possible to assign the island edges on the upper part of island 2. Specifically, considering its orientation, we can identify the bright edges of this island at this condition as (originally) Fe-edges and the adjacent darker ones as O-edges. Considering further the known orientation of the Pt(111) substrate, this means that this part of island 2 is in the favored FeO orientation. Regarding the marked edges of island 1 on the left, we note that they showed changes in the STM movie that were analogous to those observed on island 2. This and

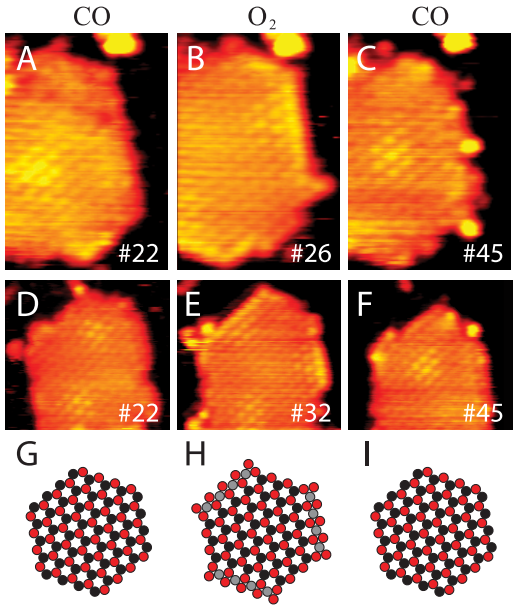

Figure 3. Zoom-in images selected from the STM movie on CO oxidation: (A–C) Island 1 (32 Å × 49 Å) and (D–F) island 2 (48 Å × 45 Å). Changes in appearance and roughness of the Fe-edges on these two islands during exposures to O_2 and CO are visible. Image numbers are given in the lower right corners. See Figure 2 for the detailed experimental conditions. (G–I) Illustration of the changes on the Fe-edges corresponding to the zoom-in STM images. Fe and O atoms are shown in black and red, respectively. Four-fold O-coordinated Fe atoms are shown in gray.

their orientations let us believe that island 1 is likewise composed from FeO in the favored orientation and that the island edges appearing bright at O-rich conditions are (originally) also Fe-edges.

In Figure 3A–C, we zoom in on island 1, and in Figure 3D–F on the upper part of island 2, considering the changes on the edges in more detail. The original Fe-edges appear brightest at O-rich conditions (see images #26 and #32 in Figure 3B and E, respectively) compared to less oxidizing or reducing conditions (see the other images in Figure 3). We attribute this finding to O_2 dissociation events at the Fe-edges, transforming them into oxidized Fe-edges, which appear brighter in STM than the original Fe-edges do.[53] Since the appearance of the Fe-edges switches back to their normal state after CO exposure, we further conclude that CO oxidation took place, leading to the removal of the O adatoms at the Fe-edges. The addition and removal of O adatoms at Fe-edges is shown schematically in Figure 3G–I.

Considering the oxidized Fe-edges in images #26 and #32 in Figure 3B and E, respectively, it is striking that these edges are straight and characterized by very few irregularities. However, under less oxidizing conditions, quite a number of irregularities are noticeable at these edges. Thus, the illustration in Figure 3G–I is a simplification. For example, comparing image #26 with image #45 (see Figure 3B,C), it is apparent that additional changes occurred at the

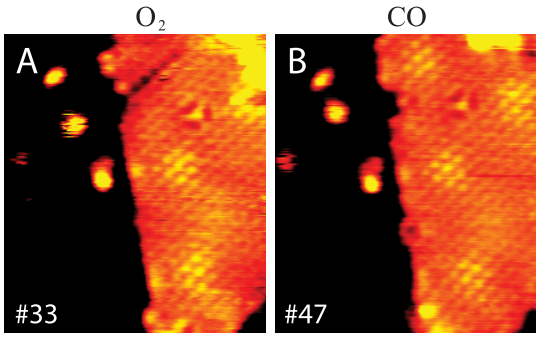

Figure 4. Zoom-in images (64 Å × 73 Å) selected from STM movie on CO oxidation: (A) O-edge on island 2 under O-rich conditions. (B) Exposing the FeO_{is}/Pt(111) sample to CO did not lead to significant changes at the O-edge. Note that the moiré domains stayed the same in the two STM images (compare the bright top domains in the lower half of the STM images).

Fe-edges upon CO oxidation, leading to a roughening of the Fe-edges.

The formation of oxidized Fe-edges is accompanied by a shift of the islands such that the bright top domains sit at these new edges (see images #26 and #32 in Figure 3B and E, respectively). This is further indication, in addition to the "brightening", that the edge termination has changed. It is rather difficult to conclude from the STM images whether or not the whole island has changed the FeO orientation, but the assignments of the edges are only consistent with our previous results[53] if we assume that the FeO orientation stayed the same. Accordingly, we exclude a switching of the FeO orientation upon oxidation of the Fe-edges.

Finally, we consider the island edge in the lower right part of the STM images depicted in Figure 2B–D. Under O-rich conditions, this edge appeared quite bright (see image #32 in Figure 2B), which might be taken as an indication that it is an oxidized Fe-edge. However, it is more likely that this bright appearance originates from an O adatom dislocation that is running very close to the edge. In any case, under O-rich conditions in STM image #33, we find a simple O-edge at this location on island 2, which does not appear bright (see Figure 4A). Importantly, no significant changes occurred at this edge when exposing the FeO_{is}/Pt(111) sample again to CO (see Figure 4B), indicating that the O-edges are unreactive at RT. Note also that the moiré domains stayed the same in the two STM images presented in Figure 4 and that the top domains are sitting away from the edges, unlike that observed on the oxidized Fe-edges (see Figure 3B,E).

DFT Results. To deepen our understanding of the CO oxidation at the FeO–Pt(111) interface, we have carried out DFT+U calculations, using the VASP code[69,70] based on spin-polarized density functional theory and the DFT+U approach by Dudarev et al.[71] We modeled the FeO–Pt(111) interface by using an FeO ribbon,

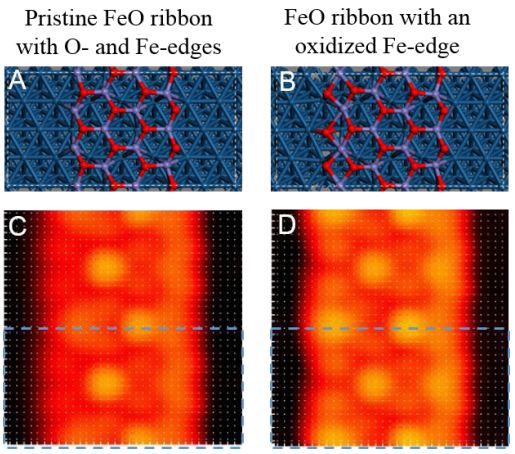

Figure 5. (A) Atomic-scale structure of a pristine FeO ribbon adsorbed on Pt(111). (B) Atomic-scale structure of a FeO ribbon with an oxidized Fe-edge on the left. Pt, Fe, and O atoms are shown in blue, violet, and red, respectively. (C) Simulated STM image of a pristine FeO ribbon on Pt(111). (D) Simulated STM image of a FeO ribbon with an oxidized Fe-edge. A bias of +0.65 V was used to simulate these STM images. The dashed rectangles in (C) and (D) indicate the supercell of (A) and (B), respectively.

consisting of 4 Fe columns, that is adsorbed on the Pt(111) substrate (see Figure 5). Figure 5A shows the optimized structure of a pristine FeO ribbon, and the optimized structure of a FeO-ribbon with an oxidized Fe-edge is depicted in Figure 5B. The pristine FeO ribbon is terminated on the left by a Fe-edge (comprising CUF sites) and on the right by an O-edge. Oxidized Fe-edges of the FeO–Pt(111) interface are created by letting O_2 dissociate at Fe-edges of pristine FeO islands, a process which is very facile.[10,49–52] Accordingly, when modeling the FeO–Pt(111) interface with oxidized Fe-edges, the difference to the pristine FeO-ribbon is the row of additional O atoms on the Fe-edges on the left (see Figure 5B). *Via* the addition of the O atoms, originally 2-fold coordinated Fe atoms are transformed into 4-fold coordinated Fe atoms.

The computed heights of the Fe atoms in the FeO ribbons relative to the topmost Pt layer are compiled in Table 1. Compared to the Fe atoms at fcc and hcp domains, the Fe atoms at top domains are characterized by larger relative heights. This is true for both considered FeO ribbons and very similar to the case of a full FeO layer on Pt(111).[55] Comparing the relative heights of the Fe atoms in the pristine FeO ribbon (Table 1A) with those of the FeO-ribbon with an oxidized Fe-edge (Table 1B) we found noticeable differences exclusively at the left side, that is, at the Fe-edge, where the structures differ from each other. Specifically, the height of the Fe atom at the top domain of the FeO-ribbon with an oxidized Fe-edge is smaller by 0.07 Å, whereas the heights of the Fe atoms in the fcc and hcp domains are higher by 0.16 and 0.23 Å, respectively.

Applying the Tersoff–Hamann approximation,[72] we simulated STM images of the considered FeO

TABLE 1. Relative Heights of Fe Atoms, δz[a]

(A) pristine FeO ribbon

at Fe-edge		next to Fe-edge		next to O-edge		at O-edge	
domain	δz	domain	δz	domain	δz	domain	δz
top	2.47	fcc	2.29	top	2.58	fcc	2.31
hcp	2.10	top	2.63	hcp	2.30	top	2.66
fcc	2.07	hcp	2.31	fcc	2.29	hcp	2.32

(B) FeO ribbon with an oxidized Fe-edge

at oxidized Fe-edge		next to oxidized Fe-edge		next to O-edge		at O-edge	
domain	δz	domain	δz	domain	δz	domain	δz
top	2.40	fcc	2.31	top	2.59	fcc	2.30
hcp	2.26	top	2.61	hcp	2.32	top	2.67
fcc	2.30	hcp	2.34	fcc	2.31	hcp	2.33

[a] (A) Relative heights of Fe atoms, δz, with respect to the topmost Pt layer in the case of a pristine FeO ribbon on Pt(111). See Figure 5A for the positions of the Fe atoms. (B) Relative heights of Fe atoms, δz, in the case of an FeO ribbon with an oxidized Fe-edge. See Figure 5B for the positions of the Fe atoms. All relative heights are given in Å.

ribbons at a bias of +650 mV (see Figure 5C,D). At this condition, Fe atoms are imaged brighter than O atoms. The Fe-edge (left boundary of the pristine FeO ribbon, see Figure 5C) appears relatively dark; the apparent height of the Fe atoms on the top domain at the Fe-edge is much lower than that of Fe atoms on the top domains at other places. In fact, in the simulated STM image of the pristine FeO ribbon, the O-edge appears brighter than the Fe-edge. However, the oxidized Fe-edge (left boundary of the FeO ribbon on the right, see Figure 5D) appears brighter than the Fe-edge and also brighter than the O-edge.

How bright the Fe atoms appear in the simulated STM images does not only depend on their heights with respect to the topmost Pt layer. For example, at the FeO ribbon with the oxidized Fe-edge (see Figure 5B) the relative heights of the Fe atoms at the top sites were found to be 2.40, 2.61, 2.59, and 2.67 Å, respectively (from left to right, see Table 1B). The relative height of the Fe atom directly at the oxidized Fe-edge (2.40 Å) is the lowest compared to all other Fe atoms at top sites. Nevertheless, the Fe atoms at the top sites appear brightest in the simulated STM images.

To examine the catalytic activity toward CO oxidation, we have modeled CO oxidation reaction pathways at the FeO−Pt(111) interface, considering both oxidized Fe-edges and simple O-edges (see Figures 6 and 7). Starting with the oxidized Fe-edge (Figure 6), we found that an adsorbed CO molecule at the bridge site [Figure 6A, CO(B2)] can easily diffuse to the top site [Figure 6B, CO(T2)], because the energy barrier for this process is only 0.25 eV. When the CO molecule is adsorbed on the top side [CO(T2)] it can react with

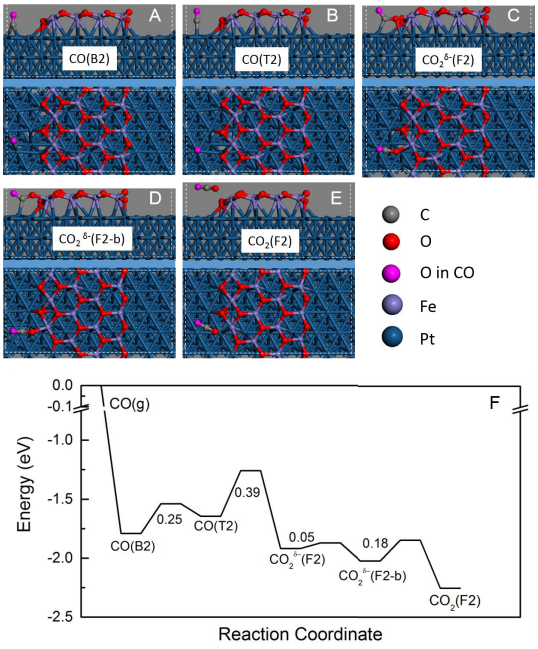

Figure 6. (A−E) DFT-based atomic structures of the intermediates in the CO oxidation reaction at the oxidized Fe-edge at the FeO−Pt(111) interface. (F) Potential energy curve for the CO oxidation at the oxidized Fe-edge. The corresponding configurations and the barrier heights are indicated.

the nearby O atom at the FeO−Pt(111) interface, forming chemisorbed CO_2 [Figure 6C, $CO_2^{\delta-}$(F2)]. The energy barrier for this process is calculated to be 0.39 eV. The formed CO_2 molecule [$CO_2^{\delta-}$(F2)] subsequently diffuses to a slightly more stable chemisorbed state [Figure 6D, $CO_2^{\delta-}$(F2-b)], a process which is very facile since its energy barrier is negligible. Finally, the chemisorbed CO_2 molecule [$CO_2^{\delta-}$(F2-b)] desorbs from the surface, ending with CO_2 weakly physisorbed above the surface [Figure 6E, CO_2(F2)]. This desorption process is hindered by a small energy barrier (0.18 eV).

Figure 6F shows the calculated potential energy surface for the CO oxidation reaction at the oxidized Fe-edge. It can be seen that the reaction is exothermic, with a reaction energy of −2.25 eV. In addition, the reaction should be very facile, since the barrier of the rate-determining step [CO(T2) → $CO_2^{\delta-}$(F2)] was found to be only 0.39 eV.

Next we examined the CO oxidation reaction at an O-edge; see Figure 7. As in the case of reaction on the oxidized Fe-edge, a CO molecule first diffuses from the bridge site [Figure 7A, CO(B5)] to the top site [Figure 7B, CO (T5)], which lies closer to the O-edge at the FeO−Pt(111) interface. This process is hindered by an energy barrier of 0.27 eV (see Figure 7E). Subsequently, the actual CO oxidation reaction may occur, when the CO molecule [CO(T5)] reacts with a neighboring O atom of the O-edge, forming chemisorbed CO_2, see Figure 7C, $CO_2^{\delta-}$(F5). The reaction barrier for this process was

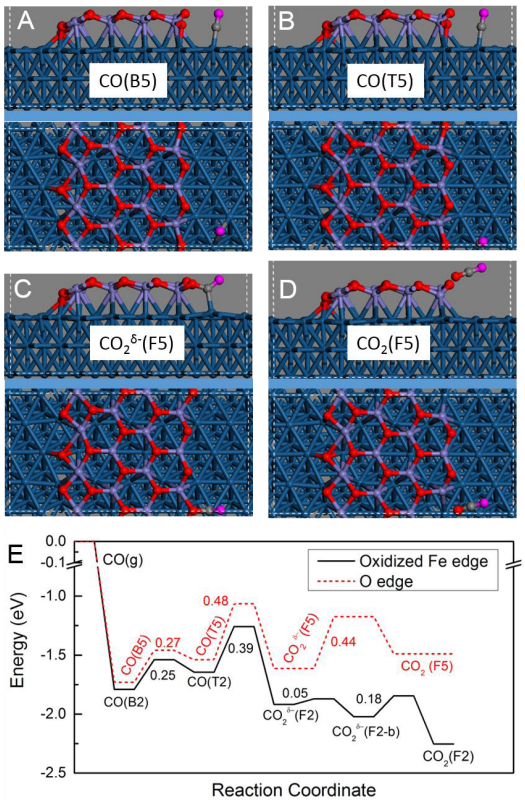

Figure 7. (A–D) DFT-based atomic structures of the intermediates in the CO oxidation reaction at the O-edge at the FeO–Pt(111) interface. The same color code is used as in Figure 6. (E) Potential energy curve for the CO oxidation at the O-edge (red, dotted line). The corresponding configurations and the barrier heights are indicated. For direct comparison, the potential energy curve for the CO oxidation at the oxidized Fe-edge is also plotted (black line).

computed to be 0.48 eV. To complete the reaction, the bond between the C of the CO_2 molecule [$CO_2^{\delta-}$(F5)] and the Pt atom and the bonds between the reactive O and Fe need to be broken, a process which is hindered by a barrier of 0.44 eV.

As can be seen from Figure 7E, the CO oxidation at the O-edge on the FeO–Pt(111) interface is exothermic by −1.49 eV. Accordingly, at the O-edge the CO oxidation reaction is 0.76 eV less favorable than at the oxidized Fe-edge. The energy barrier of the rate-determining step at the O-edge, CO(T5) → $CO_2^{\delta-}$(F5), is 0.48 eV, which is 0.09 eV higher in energy than the barrier of the corresponding rate-determining step, CO(T2) → $CO_2^{\delta-}$(F2), at the oxidized Fe-edge. Clearly, oxidized Fe-edges are more reactive in the CO oxidation than O-edges.

DISCUSSION

The presented *in situ* STM data (Figures 2, 3, STM movie on CO oxidation, and an additional STM data set in the Supporting Information) show directly that the oxidized Fe-edges are reactive in the CO oxidation reaction at RT. This is an important result since, regarding the reactivity, previous reports on FeO_{is}/Pt(111) relied on an averaging technique in conjunction with DFT calculations,[10] or exclusively on DFT calculations.[49−52] The actual evidence that the catalytically active sites are the CUF sites was still lacking. Because the used substrate, Pt(111), is itself a catalytically active system, averaging techniques may be misleading and not be considered as absolutely conclusive. Nevertheless, we found direct evidence by STM for the proposed high catalytic activity of the CUF sites, strongly supporting the conclusions put forward by Fu et al. in ref 10.

Furthermore, our direct view on the FeO_{is}/Pt(111) model catalyst revealed that the FeO–Pt(111) interface is not composed exclusively of CUF sites, as originally anticipated. Instead, Fe-edges and O-edges alternate on pristine FeO islands and their lengths depends on the preparation conditions.[53] This result implies that the CUF sites are, on a per site basis, even more reactive than previously thought.[10] Whereas STM evidence for activity in the CO oxidation reaction at oxidized Fe-edges was found at RT, the O-edges did not show characteristic changes at the same conditions (see Figure 4), suggesting that they are much less reactive, or unreactive.

The basis for the *in situ* observation of catalytic activity at the oxidized Fe-edges lies in the possibility to distinguish between bare and oxidized Fe-edges in STM. This possibility is related to the fact that the heights of the Fe atoms with respect to the topmost Pt layer depend critically on how highly the Fe atoms are O-coordinated. Generally, the higher the coordination of Fe atoms to O atoms the larger is the distance between Fe and Pt atoms (see Table 1). In the used tip state and the applied scanning conditions, this led to a brighter appearance of the oxidized Fe-edges in the STM images. Considering that the tip state plays a strong role in STM imaging, simulated STM images such as the ones shown in Figure 5C,D need to be treated with caution. Nevertheless, the simulated STM images reflect the main features of the experimental STM images quite well. Regarding the bright appearance of the oxidized Fe-edges we further note that the O adatom dislocations on FeO_{is}/Pt(111)[53] and continuous FeO films on Pd(111),[73] which show the same structural arrangements (including 4-fold coordinated Fe atoms) as oxidized Fe-edges, also appear very bright in the STM images. Notice that the only difference between O adatom dislocations and oxidized Fe-edges is that the latter are located at the islands boundaries, whereas O adatom dislocations occur on the FeO islands and continuous FeO films.

The results of our DFT+U calculations are in very good agreement with the presented STM results. The computed energy barrier of 0.39 eV for the CO oxidation at the oxidized Fe-edges is sufficiently low for reactions to occur at RT, as observed experimentally. Furthermore, the DFT+U calculations revealed that the

CO oxidation reaction at the oxidized Fe-edges is both thermodynamically and kinetically more favorable than on the O-edges. Also this result is in good accord with the experimental results, although a reaction barrier of 0.48 eV for the CO oxidation reaction at the O-edges seems not impossible to overcome at RT. Comparing our DFT+U calculations with previous DFT results,[49,50] there is generally good agreement. However, Sun et al.[50] reported a reaction barrier of only 0.2 eV for the CO oxidation at the oxidized Fe-edges, which is about half as high as ours of 0.39 eV. We believe that this discrepancy is largely related to the ways how the FeO−Pt(111) interface was modeled. For example, whereas a FeO ribbon consisting of 4 Fe columns and 4 O columns was used here, Sun et al. modeled the FeO−Pt(111) interface by means of a FeO ribbon consisting of 3 Fe columns and 2 O columns. A more detailed discussion of the DFT models and the DFT+U calculations will be presented in a separate publication.

CONCLUSIONS

In summary, by means of *in situ* STM measurements, we have obtained direct evidence that oxidized Fe-edges at the FeO−Pt(111) interface are active sites for the CO oxidation reaction at Pt(111)-supported ultrathin FeO islands. This was achieved by scanning in a tip state in which original Fe-edges and oxidized Fe-edges (characterized by a row of O adatoms off the Fe-edge) can be distinguished on the basis of their apparent STM heights. We conclude that CO oxidation occurred at the oxidized Fe-edges at RT, because the appearance of the Fe-edges was reversible, depending on whether the gas environment in the tunnel junction was oxidizing (O_2) or reducing (CO). Whereas the CO oxidation reaction occurred at the oxidized Fe-edges at RT, no sign for a reaction was found at the O-edges at identical condition. These results strongly support the high catalytic activity of the CUF sites at the FeO−Pt(111) interface and represent a very scarce example for direct insight into catalytic activity occurring at an interface.

METHODS

Experimental Details. The STM experiments were performed in a UHV chamber with a base pressure of $\sim 1 \times 10^{-10}$ mbar equipped with a home-built, variable-temperature Aarhus scanning tunneling microscope,[74,75] an electron-beam evaporator (Oxford Applied Research, EGCO4), and standard facilities for sample cleaning and preparation. The Pt(111) sample was cleaned by cycles of Ar^+-sputtering at RT and vacuum-annealing at temperatures up to ~1100 K. When needed, the sample was annealed in 5×10^{-8} mbar O_2 at 850 K to oxidize any carbon species on the surface. FeO islands covering ~25% of the surface were grown by reactive deposition of Fe (Goodfellow, 99.99%) in a background of 1×10^{-6} mbar O_2 with the sample held at RT ["*as-prepared* FeO_{is}/Pt(111)"]. The STM measurements were carried out in the constant current mode at RT using mechanically cut Pt/Ir tips.

Computational Details. All calculations were performed using the VASP code[69,70] based on spin-polarized density functional theory and the DFT+U approach by Dudarev et al.[71] The projector augmented wave potentials[76,77] were used for describing the electron−ion interactions, and the generalized gradient approximation (GGA-PW91)[78] was used to describe the exchange-correlation functional. The electron wave function was expanded with plane waves with an energy cutoff of 400 eV. The parameters describing the on-site Coulomb interaction between Fe 3*d* orbitals were chosen as $U = 4$ eV and $J = 1$ eV ($U_{eff} = U - J = 3$ eV). To model an FeO island on Pt(111), we used a FeO(111)−(4×3) ribbon/Pt(111)−$(7 \times 2\sqrt{3})$ unit cell, with the supporting Pt(111) slab containing three layers of Pt atoms. A vacuum layer of ~12 Å was used to separate the periodically repeated images in the *z*-direction. The Brillouin zone was sampled with a $(1 \times 2 \times 1)$ k-point mesh. A row-wise antiferromagnetic (RW-AFM) ordering was used as an initial guess of the magnetic structure of the FeO island. The FeO island, adsorbates, and the top Pt layer were fully relaxed, whereas the two Pt layers at the bottom were kept fixed. All structures were relaxed until the Hellmann−Feynman forces on nonfixed atoms were smaller than 0.02 eV/Å. The optimized Pt lattice constant of 3.99 Å was used, corresponding to a Pt−Pt spacing of 2.82 Å in the (111) plane. This lattice constant is in good agreement with the experimentally determined lattice constant for Pt (3.92 Å).[79] The climbing image nudged elastic band (CI-NEB) method[80] was used to calculate the activation energy barriers for the CO oxidation, with the transition states verified through a rigorous vibrational frequency analysis.

Conflict of Interest: The authors declare no competing financial interest.

Acknowledgment. We acknowledge with thanks the support of this work by the Danish Research Agency, the Strategic Research Council, the Villum Kahn Rasmussen Foundation, the Carlsberg Foundation, and the European Research Council through an Advanced ERC grant (F.B.). Work at UW—Madison was supported by DOE-BES, Division of Chemical Sciences (Grant DE-FG02-05ER15731), and by the Air Force Office of Scientific Research under a Basic Research Initiative grant (AFOSR FA9550-12-1-0481). Supercomputer time at National Energy Research Scientific Computing Center (NERSC), Pacific Northwest National Laboratory (PNNL), and Argonne National Laboratory (ANL), all supported by the DOE, is greatly appreciated. Additional CPU resources at the DoD High Performance Computing Modernization Program (U.S. Air Force Research Laboratory DoD Supercomputing Resource Center (AFRL DSRC), the U.S. Army Engineer Research and Development Center (ERDC), and the Navy DoD Supercomputing Resource Center (Navy DSRC)) supported by the Department of Defense, were used to conduct this work.

Supporting Information Available: STM movie on CO oxidation, enlarged STM images of the main article without symbols, and an additional STM data set that illustrates the changes at the FeO−Pt(111) interface and on the FeO islands, occurring when a CO-exposed FeO_{is}/Pt(111) sample is exposed to O_2 at RT. The Supporting Information is available free of charge on the ACS Publications website at DOI: 10.1021/acsnano.5b02339.

REFERENCES AND NOTES

1. Chen, M. S.; Cal, Y.; Yan, Z.; Gath, K. K.; Axnanda, S.; Goodman, D. W. Highly Active Surfaces for CO Oxidation on Rh, Pd, and Pt. *Surf. Sci.* **2007**, *601*, 5326–5331.
2. Over, H. Surface Chemistry of Ruthenium Dioxide in Heterogeneous Catalysis and Electrocatalysis: From Fundamental to Applied Research. *Chem. Rev.* **2012**, *112*, 3356–3426.

3. Weaver, J. F. Surface Chemistry of Late Transition Metal Oxides. *Chem. Rev.* **2013**, *113*, 4164–4215.
4. Vattuone, L.; Savio, L.; Rocca, M. Bridging the Structure Gap: Chemistry of Nanostructured Surfaces at Well-Defined Defects. *Surf. Sci. Rep.* **2008**, *63*, 101–168.
5. Zambelli, T.; Wintterlin, J.; Trost, J.; Ertl, G. Identification of the "Active Sites" of a Surface-Catalyzed Reaction. *Science* **1996**, *273*, 1688–1690.
6. Dahl, S.; Logadottir, A.; Egeberg, R. C.; Larsen, J. H.; Chorkendorff, I.; Tornqvist, E.; Nørskov, J. K. Role of Steps in N_2 Activation on Ru(0001). *Phys. Rev. Lett.* **1999**, *83*, 1814–1817.
7. Helveg, S.; Lauritsen, J. V.; Lægsgaard, E.; Stensgaard, I.; Nørskov, J. K.; Clausen, B. S.; Topsøe, H.; Besenbacher, F. Atomic-Scale Structure of Single-layer MoS_2 Nanoclusters. *Phys. Rev. Lett.* **2000**, *84*, 951–954.
8. Honkala, K.; Hellman, A.; Remediakis, I. N.; Logadottir, A.; Carlsson, A.; Dahl, S.; Christensen, C. H.; Nørskov, J. K. Ammonia Synthesis from First-Principles Calculations. *Science* **2005**, *307*, 555–558.
9. Wang, J. G.; Li, W. X.; Borg, M.; Gustafson, J.; Mikkelsen, A.; Pedersen, T. M.; Lundgren, E.; Weissenrieder, J.; Klikovits, J.; Schmid, M.; Hammer, B.; Andersen, J. N. One-Dimensional PtO_2 at Pt Steps: Formation and Reaction with CO. *Phys. Rev. Lett.* **2005**, *95*, 256102.
10. Fu, Q.; Li, W.-X.; Yao, Y.; Liu, H.; Su, H.-Y.; Ma, D.; Gu, X.-K.; Chen, L.; Wang, Z.; Zhang, H.; Wang, B.; Bao, X. Interface-Confined Ferrous Centers for Catalytic Oxidation. *Science* **2010**, *328*, 1141–1144.
11. Qiao, B. T.; Wang, A. Q.; Yang, X. F.; Allard, L. F.; Jiang, Z.; Cui, Y. T.; Liu, J. Y.; Li, J.; Zhang, T. Single-Atom Catalysis of CO Oxidation Using Pt_1/FeO_x. *Nat. Chem.* **2011**, *3*, 634–641.
12. Behrens, M.; Studt, F.; Kasatkin, I.; Kuhl, S.; Hävecker, M.; Abild-Pedersen, F.; Zander, S.; Girgsdies, F.; Kurr, P.; Kniep, B. L.; Tovar, M.; Fischer, R. W.; Nørskov, J. K.; Schlögl, R. The Active Site of Methanol Synthesis over $Cu/ZnO/Al_2O_3$ Industrial Catalysts. *Science* **2012**, *336*, 893–897.
13. Chen, G. X.; Zhao, Y.; Fu, G.; Duchesne, P. N.; Gu, L.; Zheng, Y. P.; Weng, X. F.; Chen, M. S.; Zhang, P.; Pao, C. W.; Lee, J. F.; Zheng, N. F. Interfacial Effects in Iron-Nickel Hydroxide-Platinum Nanoparticles Enhance Catalytic Oxidation. *Science* **2014**, *344*, 495–499.
14. Besenbacher, F.; Chorkendorff, I.; Clausen, B. S.; Hammer, B.; Molenbroek, A. M.; Nørskov, J. K.; Stensgaard, I. Design of a Surface Catalyst for Steam Reforming. *Science* **1998**, *279*, 1913–1914.
15. Gambardella, P.; Sljivancanin, Z.; Hammer, B.; Blanc, M.; Kuhnke, K.; Kern, K. Oxygen Dissociation at Pt Steps. *Phys. Rev. Lett.* **2001**, *87*, 056103.
16. Xu, Y.; Mavrikakis, M. Adsorption and Dissociation of O_2 on Gold Surfaces: Effect of Steps and Strain. *J. Phys. Chem. B* **2003**, *107*, 9298–9307.
17. Hendriksen, B. L. M.; Ackermann, M. D.; van Rijn, R.; Stoltz, D.; Popa, I.; Balmes, O.; Resta, A.; Wermeille, D.; Felici, R.; Ferrer, S.; Frenken, J. W. M. The Role of Steps in Surface Catalysis and Reaction Oscillations. *Nat. Chem.* **2010**, *2*, 730–734.
18. Rodriguez, J. A.; Ma, S.; Liu, P.; Hrbek, J.; Evans, J.; Perez, M. Activity of CeO_x and TiO_x Nanoparticles Grown on Au(111) in the Water-Gas Shift Reaction. *Science* **2007**, *318*, 1757–1760.
19. Green, I. X.; Tang, W. J.; Neurock, M.; Yates, J. T., Jr. Spectroscopic Observation of Dual Catalytic Sites During Oxidation of CO on a Au/TiO_2 Catalyst. *Science* **2011**, *333*, 736–739.
20. Saavedra, J.; Doan, H. A.; Pursell, C. J.; Grabow, L. C.; Chandler, B. D. The Critical Role of Water at the Gold-Titania Interface in Catalytic CO Oxidation. *Science* **2014**, *345*, 1599–1602.
21. Somorjai, G. A. *Introduction to Surface Chemistry and Catalysis*, 1st ed.; John Wiley and Sons: New York, 1994; p 694.
22. Freund, H.-J.; Goodman, D. W. Ultrathin Oxide Films. In *Handbook of Heterogeneous Catalysis*; Ertl, G., Knözinger, H., Schüth, F., Weitkamp, J., Eds.; Wiley-VCH: New York, 2008; Vol. 8, pp 1309−1338.
23. Ertl, G. Reactions at surfaces: From atoms to complexity (Nobel lecture). *Angew. Chem., Int. Ed.* **2008**, *47*, 3524–3535.
24. Wintterlin, J.; Völkening, S.; Janssens, T. V. W.; Zambelli, T.; Ertl, G. Atomic and Macroscopic Reaction Rates of a Surface-Catalyzed Reaction. *Science* **1997**, *278*, 1931–1934.
25. Sachs, C.; Hildebrand, M.; Völkening, S.; Wintterlin, J.; Ertl, G. Spatiotemporal Self-Organization in a Surface Reaction: From the Atomic to the Mesoscopic Scale. *Science* **2001**, *293*, 1635–1638.
26. Over, H.; Knapp, M.; Lundgren, E.; Seitsonen, A. P.; Schmid, M.; Varga, P. Visualization of Atomic Processes on Ruthenium Dioxide Using Scanning Tunneling Microscopy. *ChemPhysChem* **2004**, *5*, 167–174.
27. Besenbacher, F.; Lauritsen, J. V.; Linderoth, T. R.; Lægsgaard, E.; Vang, R. T.; Wendt, S. Atomic-Scale Surface Science Phenomena Studied by Scanning Tunneling Microscopy. *Surf. Sci.* **2009**, *603*, 1315–1327.
28. Mitsui, T.; Rose, M. K.; Fomin, E.; Ogletree, D. F.; Salmeron, M. Water Diffusion and Clustering on Pd(111). *Science* **2002**, *297*, 1850–1852.
29. Mitsui, T.; Rose, M. K.; Fomin, E.; Ogletree, D. F.; Salmeron, M. Dissociative Hydrogen Adsorption on Palladium Requires Aggregates of Three or More Vacancies. *Nature* **2003**, *422*, 705–707.
30. Vestergaard, E. K.; Vang, R. T.; Knudsen, J.; Pedersen, T. M.; An, T.; Lægsgaard, E.; Stensgaard, I.; Hammer, B.; Besenbacher, F. Adsorbate-Induced Alloy Phase Separation: A Direct View by High-Pressure Scanning Tunneling Microscopy. *Phys. Rev. Lett.* **2005**, *95*, 126101.
31. Matthiesen, J.; Hansen, J. Ø.; Wendt, S.; Lira, E.; Schaub, R.; Lægsgaard, E.; Besenbacher, F.; Hammer, B. Formation and Diffusion of Water Dimers on Rutile TiO_2(110). *Phys. Rev. Lett.* **2009**, *102*, 226101.
32. Matthiesen, J.; Wendt, S.; Hansen, J. Ø.; Madsen, G. K. H.; Lira, E.; Galliker, P.; Vestergaard, E. K.; Schaub, R.; Lægsgaard, E.; Hammer, B.; Besenbacher, F. Observation of All the Intermediate Steps of a Chemical Reaction on an Oxide Surface by Scanning Tunneling Microscopy. *ACS Nano* **2009**, *3*, 517–526.
33. Merte, L. R.; Peng, G. W.; Bechstein, R.; Rieboldt, F.; Farberow, C. A.; Grabow, L. C.; Kudernatsch, W.; Wendt, S.; Lægsgaard, E.; Mavrikakis, M.; Besenbacher, F. Water-Mediated Proton Hopping on an Iron Oxide Surface. *Science* **2012**, *336*, 889–893.
34. Parkinson, G. S.; Novotny, Z.; Argentero, G.; Schmid, M.; Pavelec, J.; Kosak, R.; Blaha, P.; Diebold, U. Carbon Monoxide-Induced Adatom Sintering in a $Pd\text{-}Fe_3O_4$ Model Catalyst. *Nat. Mater.* **2013**, *12*, 724–728.
35. Savio, L.; Giallombardo, C.; Vattuone, L.; Kokalj, A.; Rocca, M. Tuning the Stoichiometry of Surface Oxide Phases by Step Morphology: Ag(511) Versus Ag(210). *Phys. Rev. Lett.* **2008**, *101*, 266103.
36. Martinez, U.; Hansen, J. Ø.; Lira, E.; Kristoffersen, H. H.; Huo, P.; Bechstein, R.; Lægsgaard, E.; Besenbacher, F.; Hammer, B.; Wendt, S. Reduced Step Edges on Rutile TiO_2(110) as Competing Defects to Oxygen Vacancies on the Terraces and Reactive Sites for Ethanol Dissociation. *Phys. Rev. Lett.* **2012**, *109*, 155501.
37. Lira, E.; Hansen, J. Ø.; Huo, P.; Bechstein, R.; Galliker, P.; Lægsgaard, E.; Hammer, B.; Wendt, S.; Besenbacher, F. Dissociative and Molecular Oxygen Chemisorption Channels on Reduced Rutile TiO_2(110): An STM and TPD Study. *Surf. Sci.* **2010**, *604*, 1945–1960.
38. Rieboldt, F.; Bechstein, R.; Besenbacher, F.; Wendt, S. Vicinal Rutile TiO_2 Surfaces and Their Interactions with O_2. *J. Phys. Chem. C* **2014**, *118*, 3620–3628.
39. Zhu, Z. W.; Melaet, G.; Axnanda, S.; Alayoglu, S.; Liu, Z.; Salmeron, M.; Somorjai, G. A. Structure and Chemical State of the Pt(557) Surface during Hydrogen Oxidation Reaction Studied by *in Situ* Scanning Tunneling Microscopy and X-ray Photoelectron Spectroscopy. *J. Am. Chem. Soc.* **2013**, *135*, 12560–12563.
40. Tison, Y.; Nielsen, K.; Mowbray, D. J.; Bech, L.; Holse, C.; Calle-Vallejo, F.; Andersen, K.; Mortensen, J. J.; Jacobsen, K. W.; Nielsen, J. H. Scanning Tunneling Microscopy

Evidence for the Dissociation of Carbon Monoxide on Ruthenium Steps. *J. Phys. Chem. C* **2012**, *116*, 14350–14359.
41. Setvin, M.; Hao, X. F.; Daniel, B.; Pavelec, J.; Novotny, Z.; Parkinson, G. S.; Schmid, M.; Kresse, G.; Franchini, C.; Diebold, U. Charge Trapping at the Step Edges of TiO_2 Anatase (101). *Angew. Chem., Int. Ed.* **2014**, *53*, 4714–4716.
42. Kristoffersen, H. H.; Hansen, J. Ø.; Martinez, U.; Wei, Y. Y.; Matthiesen, J.; Streber, R.; Bechstein, R.; Lægsgaard, E.; Besenbacher, F.; Hammer, B.; Wendt, S. Role of Steps in the Dissociative Adsorption of Water on Rutile TiO_2(110). *Phys. Rev. Lett.* **2013**, *110*, 146101.
43. Yao, Y. X.; Fu, Q. A.; Wang, Z.; Tan, D. L.; Bao, X. H. Growth and Characterization of Two-Dimensional FeO Nanoislands Supported on Pt(111). *J. Phys. Chem. C* **2010**, *114*, 17069–17079.
44. Schoiswohl, J.; Sock, M.; Chen, Q.; Thornton, G.; Kresse, G.; Ramsey, M. G.; Surnev, S.; Netzer, F. P. Metal Supported Oxide Nanostructures: Model Systems for Advanced Catalysis. *Top. Catal.* **2007**, *46*, 137–149.
45. Rodriguez, J. A.; Hrbek, J. Inverse Oxide/Metal Catalysts: A Versatile Approach for Activity Tests and Mechanistic Studies. *Surf. Sci.* **2010**, *604*, 241–244.
46. Surnev, S.; Fortunelli, A.; Netzer, F. P. Structure-Property Relationship and Chemical Aspects of Oxide-Metal Hybrid Nanostructures. *Chem. Rev.* **2013**, *113*, 4314–4372.
47. Fu, Q.; Yang, F.; Bao, X. H. Interface-Confined Oxide Nanostructures for Catalytic Oxidation Reactions. *Acc. Chem. Res.* **2013**, *46*, 1692–1701.
48. Mu, R. T.; Fu, Q.; Guo, X. G.; Xu, X. J.; Tan, D. L.; Bao, X. H. A Comparative Study in Structure and Reactivity of "FeO_x-on-Pt" and "NiO_x-on-Pt" Catalysts. *Sci. China Chem.* **2015**, *58*, 162–168.
49. Gu, X. K.; Ouyang, R. H.; Sun, D. P.; Su, H. Y.; Li, W. X. CO Oxidation at the Perimeters of an FeO/Pt(111) Interface and how Water Promotes the Activity: A First-Principles Study. *ChemSusChem* **2012**, *5*, 871–878.
50. Sun, D. P.; Gu, X.-K.; Ouyang, R. H.; Su, H. Y.; Fu, Q.; Bao, X. H.; Li, W.-X. Theoretical Study of the Role of a Metal-Cation Ensemble at the Oxide-Metal Boundary on CO Oxidation. *J. Phys. Chem. C* **2012**, *116*, 7491–7498.
51. Sun, D. P.; Li, W.-X. A First-Principles Study of the Structure, Electronic Properties, and Oxygen Binding of FeO/Pt(111) and FeO_2/Pt(111). *Chin. J. Catal.* **2013**, *34*, 973–978.
52. Wang, Y.; Zhang, H. M.; Yao, X. D.; Zhao, H. J. Edges of FeO/Pt(111) Interface: A First-Principle Theoretical Study. *J. Phys. Chem. C* **2013**, *117*, 1672–1676.
53. Zeuthen, H.; Kudernatsch, W.; Merte, L. R.; Ono, L. K.; Lammich, L.; Besenbacher, F.; Wendt, S. Unraveling the Edge Structures of Platinum(111)-Supported Ultrathin FeO Islands: The Influence of Oxidation State. *ACS Nano* **2015**, *9*, 573–583.
54. Weiss, W.; Ranke, W. Surface Chemistry and Catalysis on Well-Defined Epitaxial Iron-Oxide Layers. *Prog. Surf. Sci.* **2002**, *70*, 1–151.
55. Merte, L. R.; Grabow, L. C.; Peng, G.; Knudsen, J.; Zeuthen, H.; Kudernatsch, W.; Porsgaard, S.; Lægsgaard, E.; Mavrikakis, M.; Besenbacher, F. Tip-Dependent Scanning Tunneling Microscopy Imaging of Ultrathin FeO Films on Pt(111). *J. Phys. Chem. C* **2011**, *115*, 2089–2099.
56. Merte, L. R.; Knudsen, J.; Grabow, L. C.; Vang, R. T.; Lægsgaard, E.; Mavrikakis, M.; Besenbacher, F. Correlating STM Contrast and Atomic-Scale Structure by Chemical Modification: Vacancy Dislocation Loops on FeO/Pt(111). *Surf. Sci.* **2009**, *603*, L15–L18.
57. Giordano, L.; Pacchioni, G.; Goniakowski, J.; Nilius, N.; Rienks, E. D. L.; Freund, H.-J. Interplay between Structural, Magnetic, and Electronic Properties in a FeO/Pt(111) Ultrathin Film. *Phys. Rev. B* **2007**, *76*, 075416.
58. Knudsen, J.; Merte, L. R.; Grabow, L. C.; Eichhorn, F. M.; Porsgaard, S.; Zeuthen, H.; Vang, R. T.; Lægsgaard, E.; Mavrikakis, M.; Besenbacher, F. Reduction of FeO/Pt(111) Thin Films by Exposure to Atomic Hydrogen. *Surf. Sci.* **2010**, *604*, 11–20.
59. Campbell, C. T.; Ertl, G.; Kuipers, H.; Segner, J. A Molecular-Beam Investigation of the Interactions of CO with a Pt(111) Surface. *Surf. Sci.* **1981**, *107*, 207–219.
60. Campbell, C. T.; Ertl, G.; Kuipers, H.; Segner, J. A Molecular-Beam Study of the Catalytic-Oxidation of CO on a Pt(111) Surface. *J. Chem. Phys.* **1980**, *73*, 5862–5873.
61. Langmuir, I. The Mechanism of the Catalytic Action of Platinum in the Reactions $2CO + O_2 = 2CO_2$ and $2H_2 + O_2 = 2H_2O$. *Trans. Faraday Soc.* **1922**, *17*, 0621–0654.
62. Ertl, G.; Neumann, M.; Streit, K. M. Chemisorption of CO on Pt(111). Surface. *Surf. Sci.* **1977**, *64*, 393–410.
63. Pedersen, M. O.; Bocquet, M. L.; Sautet, P.; Lægsgaard, E.; Stensgaard, I.; Besenbacher, F. CO on Pt(111): Binding Site Assignment from the Interplay between Measured and Calculated STM Images. *Chem. Phys. Lett.* **1999**, *299*, 403–409.
64. Ma, T.; Fu, Q. A.; Yao, Y. X.; Cui, Y.; Tan, D. L.; Zhai, R. S.; Bao, X. H. Formation of Periodic Arrays of O Vacancy Clusters on Monolayer FeO Islands Grown on Pt(111). *Chin. J. Catal.* **2010**, *31*, 1013–1018.
65. Wintterlin, J.; Schuster, R.; Ertl, G. Existence of a "hot" Atom Mechanism for the Dissociation of O_2 on Pt(111). *Phys. Rev. Lett.* **1996**, *77*, 123–126.
66. Stipe, B. C.; Rezaei, M. A.; Ho, W. Atomistic Studies of O_2 Dissociation on Pt(111) Induced by Photons, Electrons, and by Heating. *Chem. Phys.* **1997**, *107*, 6443–6447.
67. Vurens, G. H.; Salmeron, M.; Somorjai, G. A. Structure, Composition and Chemisorption Studies of thin Ordered Iron-Oxide Films on Platinum(111). *Surf. Sci.* **1988**, *201*, 129–144.
68. Meyer, R.; Lahav, D.; Schalow, T.; Laurin, M.; Brandt, B.; Schauermann, S.; Guimond, S.; Kluner, T.; Kuhlenbeck, H.; Libuda, J.; Shaikhutdinov, S.; Freund, H.-J. CO Adsorption and Thermal Stability of Pd Deposited on a Thin FeO(111) Film. *Surf. Sci.* **2005**, *586*, 174–182.
69. Kresse, G.; Furthmüller, J. Efficient Iterative Schemes for Ab-Initio Total-Energy Calculations Using a Plane-Wave Basis Set. *Phys. Rev. B* **1996**, *54*, 11169–11186.
70. Kresse, G.; Furthmüller, J. Efficiency of Ab-Initio Total-Energy Calculations for Metals and Semiconductors Using a Plane-Wave Basis Set. *Comput. Mater. Sci.* **1996**, *6*, 15–50.
71. Dudarev, S. L.; Botton, G. A.; Savrasov, S. Y.; Humphreys, C. J.; Sutton, A. P. Electron-Energy-Loss Spectra and the Structural Stability of Nickel Oxide: An LSDA+U Study. *Phys. Rev. B* **1998**, *57*, 1505–1509.
72. Tersoff, J.; Hamann, D. R. Theory of the Scanning Tunneling Microscope. *Phys. Rev. B* **1985**, *31*, 805–813.
73. Zeuthen, H.; Kudernatsch, W.; Peng, G. W.; Merte, L. R.; Ono, L. K.; Lammich, L.; Bai, Y. H.; Grabow, L. C.; Mavrikakis, M.; Wendt, S.; Besenbacher, F. Structure of Stoichiometric and Oxygen-Rich Ultrathin FeO(111) Films Grown on Pd(111). *J. Phys. Chem. C* **2013**, *117*, 15155–15163.
74. Lauritsen, J. V.; Besenbacher, F. Model Catalyst Surfaces Investigated by Scanning Tunneling Microscopy. *Adv. Catal.* **2006**, *50*, 97–147.
75. Lægsgaard, E.; Besenbacher, F.; Mortensen, K.; Stensgaard, I. A Fully Automated, Thimble-Size Scanning Tunnelling Microscope. *J. Microsc* **1988**, *152*, 663–669.
76. Blöchl, P. E. Projector Augmented-Wave Method. *Phys. Rev. B* **1994**, *50*, 17953–17979.
77. Kresse, G.; Joubert, D. From Ultrasoft Pseudopotentials to the Projector Augmented-Wave Method. *Phys. Rev. B* **1999**, *59*, 1758–1775.
78. Perdew, J. P.; Wang, Y. Accurate and Simple Analytic Representation of the Electron-Gas Correlation Energy. *Phys. Rev. B* **1992**, *45*, 13244–13249.
79. Lide, D. R., Ed. *CRC Handbook of Chemistry and Physics*, 76th ed.; CRC Press: New York, 1996.
80. Henkelman, G.; Uberuaga, B. P.; Jónsson, H. A Climbing Image Nudged Elastic Band Method for Finding Saddle Points and Minimum Energy Paths. *J. Chem. Phys.* **2000**, *113*, 9901–9904.